

ARTICLE



The neuropeptide VIP potentiates intestinal innate type 2 and type 3 immunity in response to feeding

Maud Pascal^{1,2,3,6}, Alexander Kazakov^{4,6}, Grégoire Chevalier², Lola Dubrule¹, Julie Deyrat¹, Alice Dupin¹, Soham Saha¹, Ferdinand Jagot², Kurt Sailor¹, Sophie Dulauroy², Carine Moigneu¹, Yasmine Belkaid⁵, Gabriel Lepousez^{1,7}, Pierre-Marie Lledo^{1,7}, Christoph Wilhelm^{4,7} and Gérard Eberl^{2,7}

© The Author(s), under exclusive licence to Society for Mucosal Immunology 2022

The nervous system and the immune system both rely on an extensive set of modalities to perceive and act on perturbations in the internal and external environments. During feeding, the intestine is exposed to nutrients that may contain noxious substances and pathogens. Here we show that Vasoactive Intestinal Peptide (VIP), produced by the nervous system in response to feeding, potentiates the production of effector cytokines by intestinal type 2 and type 3 innate lymphoid cells (ILC2s and ILC3s). Exposure to VIP alone leads to modest activation of ILCs, but strongly potentiates ILCs to concomitant or subsequent activation by the inducer cytokines IL-33 or IL-23, *via* mobilization of cAMP and energy by glycolysis. Consequently, VIP increases resistance to intestinal infection by the helminth *Trichuris muris* and the enterobacteria *Citrobacter rodentium*. These findings uncover a functional neuro-immune crosstalk unfolding during feeding that increases the reactivity of innate immunity necessary to face potential threats associated with food intake.

Mucosal Immunology (2022) 15:629–641; <https://doi.org/10.1038/s41385-022-00516-9>

INTRODUCTION

Innate lymphoid cells (ILCs) are abundant in mucosal tissues, where they orchestrate inflammation and tissue repair early in response to infection, injury, or metabolic stress^{1,2}. During such perturbations, inducer cytokines are produced by myeloid and non-hematopoietic cells, which activate ILCs to express critical effector cytokines². Like T cells, 3 major types of ILCs respond either to intracellular pathogens and cellular transformation, to extracellular microbes, or to large parasites and tissue injury. However, in contrast to naïve T cells, ILCs do not need antigen-specific selection and therefore, respond promptly to perturbations, placing them upstream in the unfolding immune response.

Signals from the nervous system have recently been shown to reinforce activation of ILCs. The neuropeptide Neuromedin U (NMU), produced by the enteric nervous system (ENS), intensifies the expression of IL-5 and IL-13 by ILC2s, thereby increasing resistance to helminth infection in the intestine or the severity of allergy in the lung^{3–5}. Vasoactive intestinal peptide (VIP) has a similar effect on the expression of IL-5 by gut and by lung ILC2s in models of allergic airway inflammation^{6,7}. In contrast, calcitonin gene-related peptide (CGRP) negatively regulates the activity of ILC2s in both gut and lung^{8–10}. In the intestinal lamina propria, glial cells express peptide ligands of the RET tyrosine kinase that increase expression of IL-22 by ILC3s and resistance to dextran sodium sulfate (DSS)-induced colitis¹¹. Furthermore, the activity of

intestinal ILC3s follows a circadian rhythm encoded in the central nervous system (CNS)¹², but the nature of information transfer from the CNS to intestinal ILCs was not identified. Recently, it was shown that the circadian activity of intestinal ILC3s is indirectly dependent on VIP^{13,14}.

VIP, a member of the glucagon-secretin superfamily of peptides, is abundantly produced in the intestine in response to feeding^{15,16}. Upon binding to its receptors VIPR1 or VIPR2, VIP favors digestion through concerted actions ranging from water and electrolytes secretion, stimulation of the exocrine pancreas and intestinal motility^{17,18}. Furthermore, feeding, *via* VIP, increases the production of IL-22 by ILC3s, resulting in increased resistance to DSS-induced colitis¹⁴ and infection by the enteric pathogen *Citrobacter rodentium*¹⁹. However, in contrast to these results, it was also reported that feeding-induced VIP represses the activity of ILC3s, thereby decreasing resistance to bacterial infection but at the same time increasing the absorption of dietary lipids¹³. Altogether, these observations show that the nervous system effectively alerts the immune system *via* neuropeptides produced by local neurons, in response to feeding in the case of VIP, or other cues that remain to be determined in the case of NMU and CGRP.

In this study, we show that feeding-induced VIP strongly synergizes with IL-25 and IL-33, or with IL-1 β and IL-23, to induce cytokine production by ILC2s or ILC3s. Consequently, using mice deficient in VIPR2 in ILC2s or ILC3s, we demonstrate that feeding-

¹Institut Pasteur, Université Paris Cité, CNRS UMR 3571, Perception and Memory Unit, F-75015 Paris, France. ²Institut Pasteur, Université Paris Cité, INSERM U1224, Microenvironment and Immunity Unit, F-75015 Paris, France. ³PhD program 'Cerveau, Cognition, Comportement' (ED3C), Université Paris Sciences & Lettres, Paris, France. ⁴Immunopathology Unit, Institute of Clinical Chemistry and Clinical Pharmacology, University Hospital Bonn, University of Bonn, 53127 Bonn, Germany. ⁵Metaorganism Immunity Section, Laboratory of Immune System Biology, and NIAID Microbiome Program, National Institute of Allergy and Infectious Diseases, National Institutes of Health, Bethesda, MD 20892, USA. ⁶These authors contributed equally: Maud Pascal, Alexander Kazakov. ⁷These authors jointly supervised this work: Gabriel Lepousez, Pierre-Marie Lledo, Christoph Wilhelm, Gérard Eberl. ✉email: maud.pascal13@gmail.com; pierre-marie.lledo@pasteur.fr; gerard.eberl@pasteur.fr

Received: 29 November 2021 Revised: 8 April 2022 Accepted: 19 April 2022
Published online: 2 May 2022

induced VIP increases resistance to infection by pathogen eliciting either type 2 or type 3 responses. VIP marginally activates ILCs by itself. Rather, VIP effectively potentiates ILC, *via* increased levels of cAMP and glycolysis, for subsequent activation by inducer cytokines, as exposure of ILCs to VIP can precede activation by cytokines to maintain synergy, both *in vivo* and *in vitro*. These findings indicate that the ENS translates potential dangers associated with feeding into potentiation of ILCs, while actual activation of ILCs is induced by the danger itself *via* cytokines.

RESULTS

Intestinal ILC2s and ILC3s are equipped and positioned to respond to VIP

Intestinal ILC2s and ILC3s expressed high levels of mRNA coding for VIPR2, to levels similar to the NMU receptor NMUR1 (Fig. 1a), exceeding by a 100-fold the amounts expressed by CD4⁺ T cells (Fig. 1b, Supplementary Fig. 1). Furthermore, ILCs were positioned in close proximity to VIP⁺ nerve fibers in the mouse small intestine, as reported recently for ILC3s^{13,14}. VIP was visible in nerve fibers of the lamina propria, the submucosal and myenteric plexi, as punctuate clusters, consistent with its storage in dense-core vesicles (Fig. 1c). Thirty percent of neurons in the myenteric plexus, and more than half the neurons in the submucosal plexus expressed VIP, as shown in VIP^{Cre} × Rosa^{YFP} mice (Fig. 1d). In the lamina propria, ILC2s and ILC3s, visualized in Gata3^{GFP} and RORγt^{GFP} reporter mice, respectively, clustered in proximity to VIP⁺ neural fibers (Fig. 1e). A 3-dimensional quantification confirmed the close proximity of ILC2s and ILC3s with VIP⁺ fibers (Fig. 1f–h), indicating that ILCs expressing VIPR2 are well positioned to respond to VIP release. ILC2s and ILC3s also expressed high levels of the CGRP receptors RAMP1 and RAMP3, and were located in close proximity to CGRP⁺ fibers (Supplementary Fig. 2).

VIP and alarmins strongly synergize in the activation of ILCs

To assess how intestinal ILCs respond to VIP, we isolated ILC2s and ILC3s from the small intestine of reporter mice and cultured them with VIP and/or the inducer cytokines IL-33 and IL-23. VIP alone induced modest expression of IL-5 by ILC2s, but no IL-13 (Fig. 2a, c), reminiscent of the induction of IL-5 but not of IL-13 expression by CGRP⁹. In contrast, VIP-induced low or no expression of either IL-22 or IL-17 by ILC3s (Fig. 2b, e). Nonetheless, VIP strongly induced the expression of IL-5 by ILC2s when provided together with IL-33 or IL-25, and of IL-22 by ILC3s when provided together with IL-23 or IL-1β (Fig. 2a, b, Supplementary Fig. 3a), demonstrating synergy between the pathways mediated by VIP and the inducer cytokines. No significant effect of VIP was observed in CD4⁺ T cells (Supplementary Fig. 3b). Expression by ILCs of VIPR2 was required for this synergistic effect, as VIPR2-deficient ILC2s (isolated from VIPR2^{loxP} mice and treated with Tat-Cre protein, or ILC2^{ΔVIPR2} cells) and ILC3s (isolated from RORγt^{Cre} × VIPR2^{loxP}, or ILC3^{ΔVIPR2} mice) were unresponsive to VIP (Fig. 2d, f). Of note, the frequency and number of ILC2s and ILC3s expressing effector cytokines, at the steady state, is not altered by the absence of VIPR2 (Supplementary Fig. 4), and ILCs isolated from the colon showed a similar reactivity to VIP (Supplementary Fig. 3c).

VIPR2 activation engages adenylate cyclase- and phospholipase C/Ca²⁺-driven signaling pathways²⁰. In accordance with a critical role of cAMP in the potentiation of ILCs by VIP⁶, exposure of ILCs to both the inducer cytokines and dibutyryl-cAMP (db-cAMP), a membrane-permeable and non-hydrolysable form of cAMP, mimicked the synergistic effect of VIP with cytokines (Fig. 2a, b). Furthermore, Ca²⁺ was necessary for this synergy, as chelation of intracellular free Ca²⁺ with BAPTA-AM effectively blocked ILC activation (Fig. 2a, b). Similar pathways were induced by CGRP^{8–10}, as exposure of ILCs to both CGRP and the inducer cytokines leads to a cAMP- and Ca²⁺-dependent synergy in the expression of IL-5 by ILC2s and IL-22 by ILC3s (Supplementary Fig. 5a).

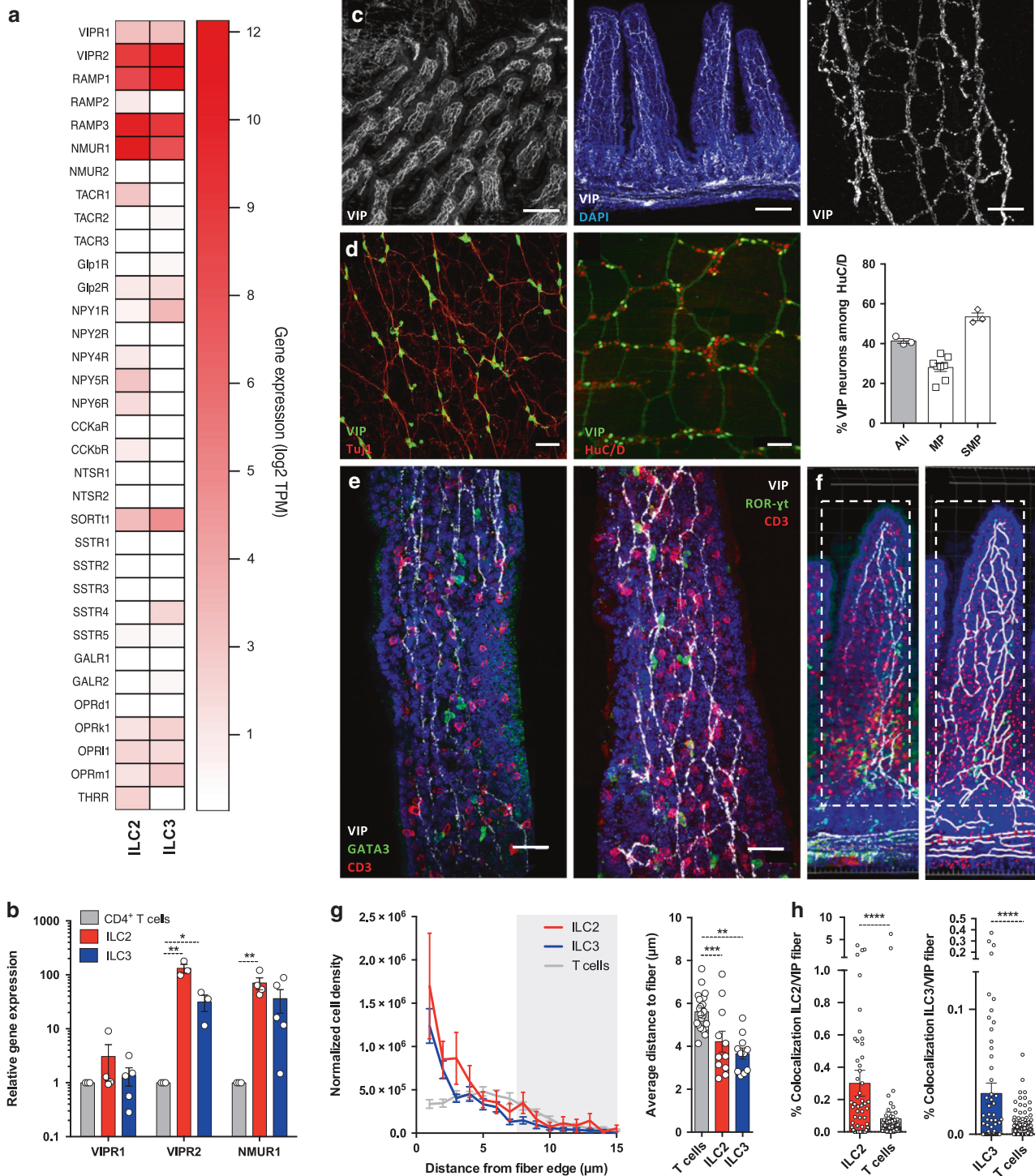
Recent reports demonstrate that proper activation of ILCs relies on mTOR activation and increased glycolysis^{21–26}. Notably, glycolysis can be induced by VIP through increased mTOR signaling^{27,28}. A transcriptional analysis was performed on ILC2s and ILC3s cultured with VIP and/or cytokines, which confirmed a VIP-mediated increase in the expression of genes promoting glycolysis (*Hif1a*, *Eno1*, *Ldha* and *Pkm*) (Fig. 2g, h). In addition, exposure of *in vivo* activated ILC2s and ILC3s to both VIP and cytokines resulted in significantly decreased phosphorylation of mTOR, AKT and S6 in VIPR2-deficient ILCs, pointing towards blunted nutrient sensing (Supplementary Fig. 5b, c). Finally, to assess the impact of VIP on ILC metabolism directly *ex vivo*, we turned to metabolism analysis using SCENITH (Single-Cell Metabolism by Profiling Translation Inhibition), a recently developed method based on the inhibition of specific metabolic pathways and the quantification of the resulting levels in protein synthesis²⁹. SCENITH revealed that, upon activation *in vivo*, wild-type but not VIPR2-deficient ILC2s and ILC3s increased their glycolytic capacity, while simultaneously reducing mitochondrial dependency (Fig. 2i, j). Together, these data indicate that VIP synergizes with inducer cytokines in the activation of ILCs through the increase in intracellular cAMP and Ca²⁺ levels, and suggest that VIP potentiates ILC function by increasing glycolysis-based energy metabolism.

Feeding induces expression of VIP by the ENS and potentiates the activation of ILCs

We next assessed whether VIP induced by feeding potentiates ILC activity. First, to determine whether feeding induces expression of VIP by neural fibers in the intestinal lamina propria, mice were fasted for 16 h before being refed *ad libitum* (Fig. 3a). After 1 h of refeeding, the expression of VIP in neuronal fibers, as well of transcript coding for VIP in total tissue, were significantly increased as compared to the expression in mice that were not refed (Fig. 3b–d). Furthermore, when mice were treated with cholecystokinin (CCK), a peptide hormone released by enteroendocrine cells of the small intestine in response to feeding, VIP was promptly (within minutes) detected in the portal vein (Fig. 3e). Altogether, these data show that feeding induces rapid VIP expression and release by the ENS, providing an early signal associated with feeding to VIPR2⁺ ILCs in the intestinal mucosa.

Lymphoid cells were then isolated from the small intestine of mice refed for 3 h, or fasted-only mice, and cultured with IL-33 or IL-23 (Supplementary Fig. 6a). In these conditions however, feeding had only a modest effect on the production of IL-5 by ILC2s, and no effect on the production of IL-22 by ILC3s (Supplementary Fig. 6b). We reasoned that the large bacterial microbiota present in the intestine may induce a predominant IL-23-mediated type 3 response in the intestinal lamina propria, and thereby repress type 2 responses mediated by ILC2s and mask re-activation of ILC3s by IL-23 *in vitro*. In agreement with this view, the levels of IL-23 in the portal vein, significantly boosted after feeding, were blunted when mice were concomitantly treated with a cocktail of antibiotics during fasting and refeeding, while levels of IL-33 were unaffected (Supplementary Fig. 6c). Lymphoid cells were thus isolated from fasted or fasted and refed mice that were concomitantly treated with antibiotics, and cultured with IL-33 or IL-23 (Fig. 4a). In such conditions, ILC2s and ILC3s expressed highly increased levels of IL-5 or IL-22 when compared to ILCs isolated from fasted-only mice (Fig. 4b). The feeding-induced increase in the production of effector cytokine was dependent on VIPR2, as ILC3^{ΔVIPR2} showed no increase in IL-22 production (Fig. 4c), while the number and frequency of ILC3s were not affected by a lack of VIPR2 expression (Supplementary Fig. 6d, e).

These data demonstrate that feeding-induced VIP increases the effector functions of ILCs upon subsequent exposure to alarmins. In addition, they suggest that VIP potentiates rather than activates ILCs, as exposure to VIP *in vivo* preceded exposure to IL-33 or IL-23 *in vitro*, while feeding and VIP alone had only a modest impact on ILCs. To demonstrate a potentiation effect of VIP on ILCs, cells



were isolated from the small intestine of untreated mice and cultured with VIP, inducer cytokines, both VIP and inducer cytokines, or sequentially with a transient VIP stimulation followed by cytokines (Fig. 4d). To temporally restrict the activation of VIPR2 and block the effects of residual VIP during exposure to cytokines, a VIPR2 antagonist was added after exposure to VIP. Effective synergy was observed when ILCs were sequentially exposed to VIP followed by cytokines, demonstrating persistent potentiation of ILC activity by VIP for at least 3 h (Fig. 4e).

Altogether, these data show that, while VIP poorly activates ILCs, VIP effectively potentiates ILC activation by inducer cytokines, even

when exposure to cytokines is delayed. This potentiation effect may be relevant in the context of feeding, where sensing of food and the rapid production of VIP (Fig. 3e) most probably precedes the impact of foodborne pathogens on tissues and the production of inducer cytokines by the host.

Feeding increases VIP and ILC-mediated resistance to intestinal infections

In the next series of experiments, we assessed whether the potentiation of ILC effector functions by VIP translates into increased resistance to (potentially foodborne) intestinal infections.

Fig. 1 ILC2s and ILC3s express VIPR2 and closely associate with VIP⁺ nerve fibers in the small intestine. **a** Heatmap for neuropeptide receptor transcripts in ILC2s and ILC3s (compounded from the Immgen database RNA-seq skyline). **b** Expression level of transcripts for VIPR1, VIPR2 and NMUR1 in ILC2s and ILC3s, relative to the expression in CD4⁺ T isolated from the intestinal lamina propria (LP). Data are from at least $n = 3$ independent experiments where cells from 5–7 mice were pooled for each data point. **c** Confocal microscopy analysis of VIP in the duodenum, with a general overview of a VIP immunostaining and a higher magnification on nerve fibers. Scale bars: 300 μm (left), 100 μm (middle) and 25 μm (right). **d** VIP gene expression, as reported in VIP^{Cre} \times Rosa^{YFP} mice, in the submucosal (left) and myenteric (right) plexus. Neuron fibers and neuron bodies were identified by Tuj1 and HuC/D⁺ staining, respectively, and neurons expressing YFP among total neurons quantified in both plexuses. Scale bars, 50 μm . **e** Confocal microscopy analysis of intestinal lamina propria CD3⁺ cells, ILC2s (left) and ILC3s (right). Scale bars, 25 μm . **f** Confocal microscopy analysis of CD3⁺ cells, ILC3s and VIP⁺ fibers on a duodenum of a ROR- γ ^{GFP} reporter mouse (left) and 3D reconstruction using the Imaris software (right). The dotted line defines the zone considered for quantification. **g** Normalized cell density as a function of the distance to the nearest VIP⁺ fiber edge measured from 3D reconstruction, and average distance of ILC2s, ILC3s or T cells to the nearest VIP⁺ fiber edge. Data are for cells location analyzed in at least $n = 10$ villi from 5 GATA3^{GFP} or ROR- γ ^{GFP} independent reporter mice. **h** Percentage of colocalization of ILC2s, ILC3s, and T cells with VIP. Data are colocalization values obtained for at least $n = 50$ cells in villi from 5 GATA3^{GFP} or ROR γ ^{GFP} reporter mice. Statistical analysis: Student's t-test. * $P < 0.05$; ** $P < 0.01$; *** $P < 0.001$; **** $P < 0.0001$; mean \pm s.e.m.

First, wild-type and ILC2 ^{Δ VIPR2} mice were infected with *Trichuris muris* and analyzed 14 days later (Fig. 5a). The caeca of ILC2 ^{Δ VIPR2} mice were significantly enlarged and harbored elevated numbers of worms (Fig. 5b, c). At the same time, the frequency and number of IL-5-expressing ILC2s were significantly reduced (Fig. 5d), as were consequently the frequencies and numbers of eosinophils (Fig. 5e). Importantly, at this stage of the immune response, only few T cells expressing IL-5 were detected in the intestine (Fig. 5f), indicating that the production of IL-5, the recruitment of eosinophils and the resistance to infection was mainly mediated by ILC2s. As *T. muris* infection may translate into IL-25 and/or IL-33 production by the host^{30,31}, we treated normally-fed mice with recombinant IL-33. Similar to the phenotype observed in the context of *T. muris* infection, the frequency of IL-5-expressing ILC2s, as well as the frequencies and numbers of eosinophils, were significantly reduced in ILC2 ^{Δ VIPR2} mice treated with IL-33 (Supplementary Fig. 7a–c). The levels of ST2, a component of the receptor for IL-33, was unaltered in ILC2s lacking VIPR2 (Supplementary Fig. 7d, e).

We then assessed the impact of VIP-mediated potentiation of ILC3s in resistance to infection by the enterobacteria *C. rodentium*, a murine homolog of attaching and effacing pathogenic human *Escherichia coli* strains. ILC3 ^{Δ VIPR2} mice and littermate controls were fasted, and concomitantly fed and gavaged with *C. rodentium*, and analyzed 4 days later at a time preceding the activation of adaptive immune responses (Fig. 5g). ILC3 ^{Δ VIPR2} mice showed significantly higher bacterial load in the stools and colon (Fig. 5h). As a consequence of the increased bacterial burden and thus, presumably, of increased levels of inducer cytokines, the number of neutrophils, as well as of IL-22-producing ILCs, was increased when measured 4 days after infection (Fig. 5i, j).

Altogether, these data show that VIP, induced by feeding, increases the resistance to colonic pathogens through the potentiation of ILC effector functions. Such effector functions are induced in ILC2s or ILC3s, depending on the nature of pathogens encountered and thus the type of inducer cytokines produced by the host.

DISCUSSION

In this study, we show that intestinal ILC2s and ILC3s express high levels of the receptors for VIP, a peptide that is released by the ENS upon food intake. VIP synergizes with the inducer cytokines IL-33 (or IL-25) and IL-23 (or IL-1 β) to induce the expression of the effector cytokines IL-5 and IL-22 by ILC2s and ILC3s, respectively. VIP is itself a poor inducer of ILC effector function, but effectively potentiates ILCs to respond to the context-dependent inducer cytokines, via the activation of the cAMP pathway and the mobilization of energy via glycolysis. Therefore, the release of intestinal VIP by neurons increases the resistance to intestinal infection by helminths through ILC2s and bacteria through ILC3s.

Three previous studies reported the modulation of ILC3 activity by VIP. Seillet et al. show that the expression of IL-22 by intestinal ILC3s is increased by exposure to VIP, leading to increased resistance to DSS-mediated colitis¹⁴. In addition, Yu et al. report that VIP promotes the recruitment of ILC3s to the intestine¹⁹. In contrast, Talbot et al. show that VIP decreases the expression of IL-22 by intestinal ILC3s, and thereby reduces resistance to infection by *C. rodentium* while increasing absorption of dietary lipids¹³. In our hands, VIP strongly synergizes with inducer cytokines in the induction of cytokine expression by ILC3s to increase resistance to *C. rodentium* infection, in agreement with a previous study showing improved VIP-mediated epithelial barrier function and consequent resistance to *C. rodentium*³². The reason for discrepancies between the studies is unclear, but the three reports use different regimen for the induction of VIP production in vivo and in vitro. Seillet et al. observe that fasting reduces ILC3 activity, and that intraperitoneal injection of VIP, or culture of ILC3s with VIP, increases their production of IL-22. Talbot et al. use ILC3 ^{Δ VIPR2} mice, a synthetic VIPR agonist and artificial DREADD-mediated inhibition of VIP⁺ neurons to show negative regulation of ILC3s by VIP. We, in contrast, used ILC3 ^{Δ VIPR2} mice, a VIPR2 antagonist, and physiological refeeding-induced VIP release, to demonstrate strong positive regulation. It is possible that the basal activation state of intestinal ILC3s in the different animal colonies is a key determinant of the impact of VIP, as we show that antibiotic treatment does unmask a positive VIP effect in vivo, and Talbot et al. report extensive colonization with Segmented Filamentous Bacteria (SFB), a potent inducer of type 3 responses^{33,34}. Also, both Seillet and Talbot report that the activity of ILC3s follows a circadian rhythm that mirrors food intake, indicating that the timing of mouse treatment and analysis may be key in the level of VIP-mediated control of ILC3 activity. Nevertheless, we have assessed different fasting and feeding protocols (Supplementary Fig. 8), at different times of day or night, as well as DREADD-induced release of VIP (Supplementary Fig. 9), to modulate ILC3s functions, but failed to observe negative regulation of ILC3s by VIP.

For technical reasons, the direct impact of VIP on ILCs has been analyzed, on ILC2s and/or ILC3s isolated from the small intestine, in this and all previous studies^{6,13,14,19}. However, challenge models have been used that target mainly the colon: the DSS-induced colitis model¹⁴, *C. rodentium* infection^{13,19} (this study) and *T. muris* infection (this study). It is possible, due to potential differences in the VIP-ILC interaction modes along the intestine, that the impact of feeding-induced VIP on ILCs differ in the small intestine and in the colon. Nevertheless, Seillet et al. showed that feeding-induced VIP expression by enteric neurons is similar in the ileum and the colon¹⁴. Furthermore, while Yu et al. and Seillet et al. use mice fully deficient in the expression of VIPR2^{14,19}, we, as well as Talbot et al., use conditional deficiency of VIPR2 in type 2 and/or type 3 lymphoid cells, mostly ILC3s and ILC2s in the time frames of

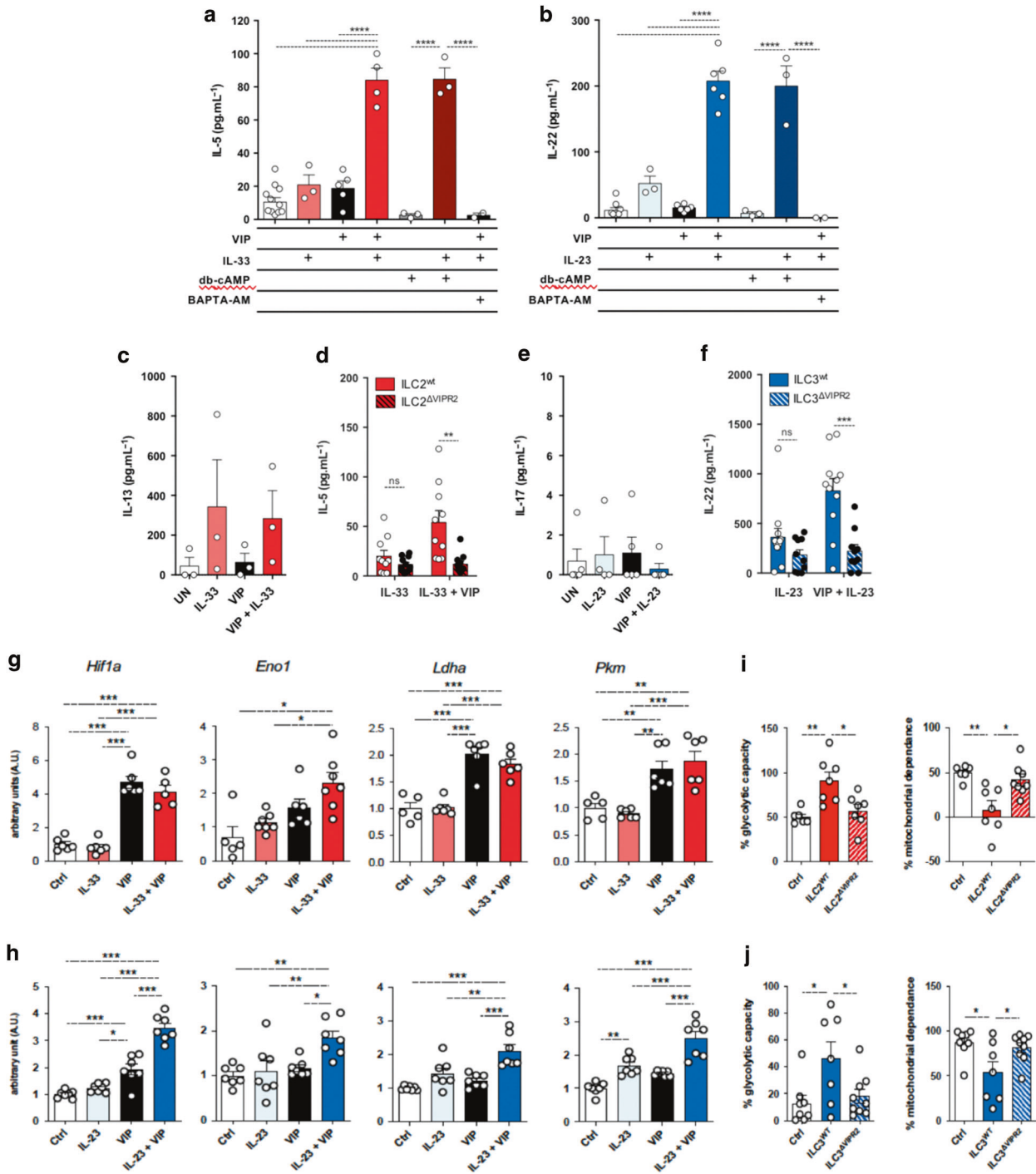


Fig. 2 VIP synergizes with alarmins to activate ILC2s and ILC3s through cAMP and Ca²⁺ dependent pathways. Production of IL-5 (a) and IL-22 (b) by 5000 FACS-sorted intestinal ILC2s or ILC3s, after 6 h of culture with different combinations of VIP, dibutyryl-cAMP (db-cAMP) and IL-33 or IL-23. BAPTA-AM was used to deplete extra and intracellular free Ca²⁺ before incubation with VIP and cytokines. Data are from at least $n = 3$ experiments where cells from 5–7 mice are pooled for each point. Production of IL-13 (c) and IL-17 (e) by FACS-sorted ILC2s or ILC3s after 6 h of culture. **d** Production of IL-5 by FACS-sorted ILC2 from wild-type (ILC2^{wt}) or VIPR2^{loxP} mice treated with Tat-Cre (ILC2^{ΔVIPR2}) after 6 h of culture. Data are from at least $n = 10$ mice and 2 experiments. **f** Production of IL-22 by FACS-sorted ILC3 isolated wild-type (ILC3^{wt}) or VIPR2^{loxP} × ROR-γt^{Cre} mice (ILC3^{ΔVIPR2}) after 6 h culture. Data are from $n = 9–10$ mice and 3 experiments. RT-PCR analysis relative to *Hprt* of flow purified ILC2s (g) and ILC3s (h) cultured with different combinations of VIP, IL-33 or IL-23 and normalized to the expression of Ctrl. Data are from $n = 3–5$ mice and 2 experiments. Control (Ctrl) and IL-33-injected ILC2^{wt} or ILC2^{ΔVIPR2} mice (i), or IL-23-injected ILC3^{wt} or ILC3^{ΔVIPR2} mice (j) were analyzed using SCENITH. Graphs show the percentage of mitochondrial dependence and glycolytic capacity of ILC2s or ILC3s. Graphs show the percentage of mitochondrial dependence and glycolytic capacity of ILC2s (i) and ILC3s (j). Data are from $n = 3–5$ mice and 2 experiments. Statistical analysis: Student's *t* test or one-way Anova (g, h). ns, not significant; ** $P < 0.01$; *** $P < 0.001$; **** $P < 0.0001$; mean ± s.e.m.

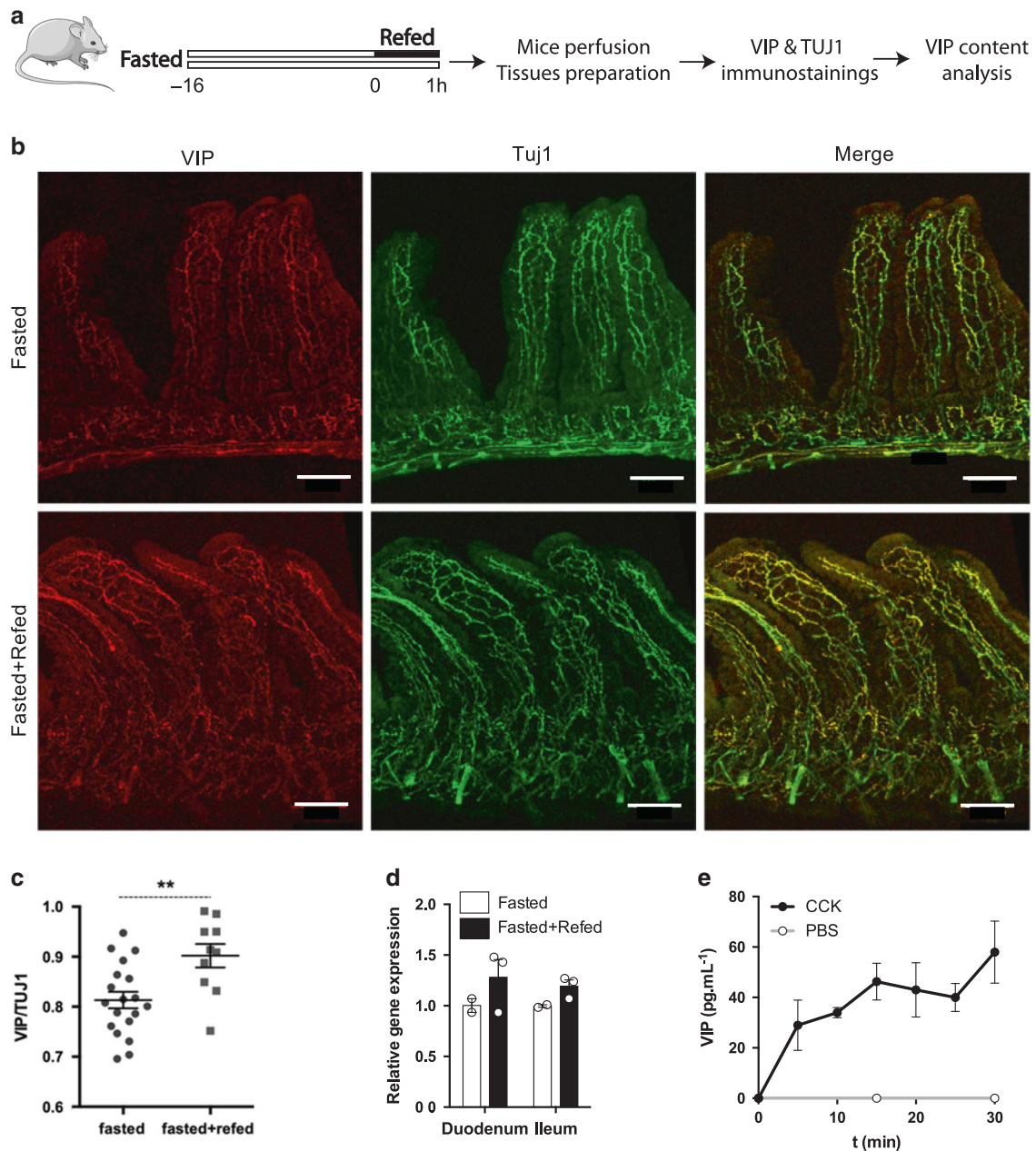


Fig. 3 Feeding induces rapid VIP release in the intestine. **a** After 16 h of fasting, one group of mice remained fasted while another group of mice was refed ad libitum during 1 h before mice were perfused and tissues prepared for analysis. **b** Representative images of VIP and Tuj1 immunostainings acquired by confocal microscopy in fasted vs fasted +1 h refed mice. Scale bars, 100 μm . **c** Quantification of the VIP content in duodenum villi nerve fibers (Tuj1) in fasted vs fasted +1 h refed mice (ratio of thresholded mean values for VIP and Tuj1 calculated for each image analyzed; each value represents one villus measurement for all the fibers contained in the imaging plane). Data are from at least $n = 10$ villi and 3 mice. **d** Level of expression of transcripts for VIP in segments of duodenum or ileum harvested from fasted or fasted +3 h refed mice. Data are from at least $n = 2$ mice. **e** Kinetic of CCK-induced VIP release in the portal vein blood. CCK was used as a temporally-controlled proxy of food intake. Data are from at least 3–4 mice from 2 independent experiments per time point. Statistical analysis: Student's t -test. ns not significant; * $P < 0.05$; ** $P < 0.01$; mean \pm s.e.m.

study¹³. Based on this experimental strategy, we show that the absence of VIPR2 expression in ILCs leads to a loss of protection against colon infections, which is in accordance with the loss of reactivity to alarmins observed in cultures of small intestine ILCs.

The increase in ILC2 activity by VIP has previously been reported in the lung, where local branches of the vagus nerve release VIP and increase the expression of IL-5 by ILC2s and Th2⁷. In turn, IL-5 increases VIP release by nerve fibers, thereby establishing a positive feedback loop in allergic reactions. VIP also induces IL-5 in

intestinal ILC2s⁶. The latter study shows that the generation and recruitment of eosinophils is induced by feeding, under control of IL-5 and IL-13 production by ILC2s, and suggests that VIP establishes a link between feeding and ILC2 activity. Our results now unequivocally demonstrate that feeding induces ILC2 expression of IL-5 via VIPR2. It may seem surprising that VIP increases the effector functions of both ILC2s and ILC3s, as type 2 and type 3 immune responses effectively antagonize each other^{35,36}. Nevertheless, as shown in our study, VIP effectively

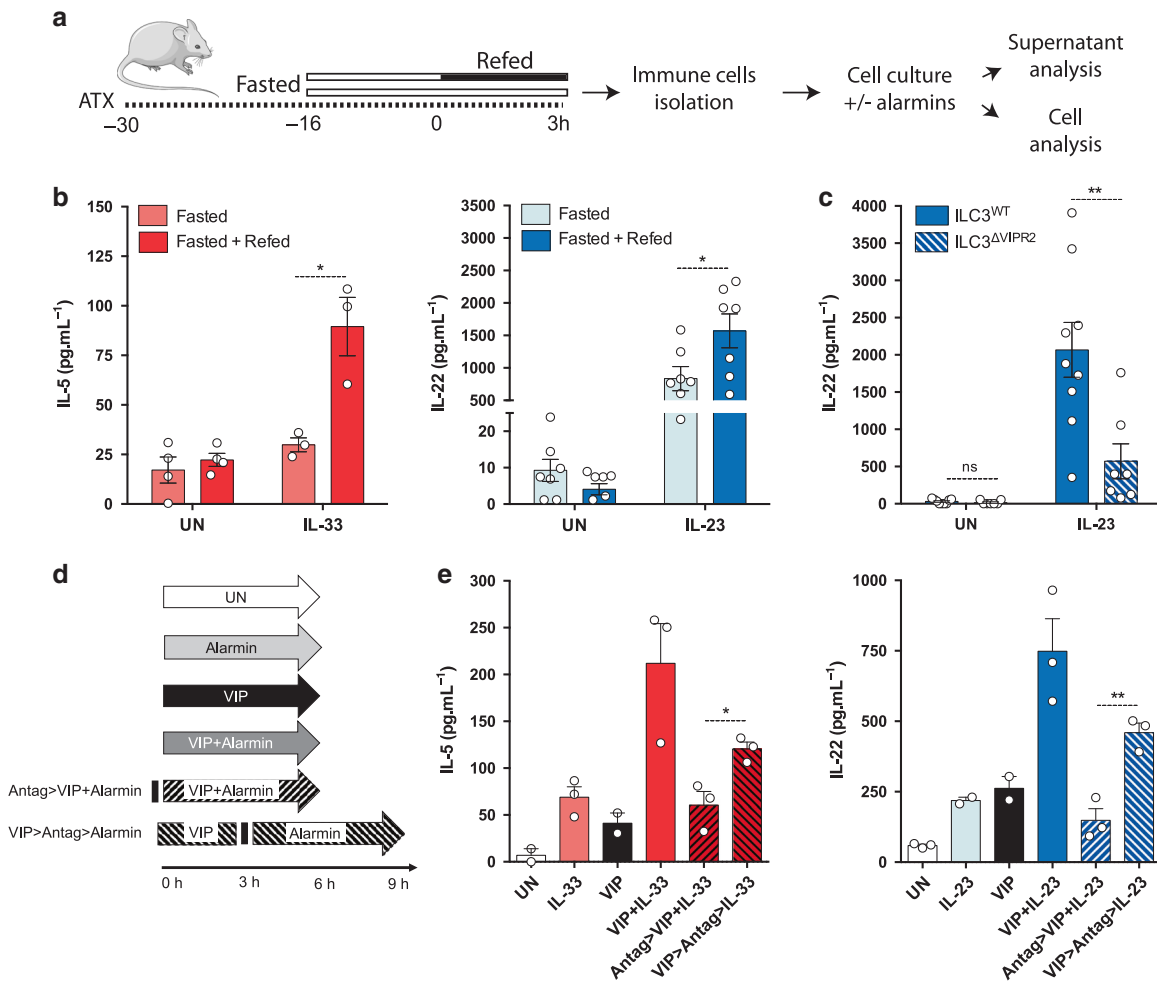


Fig. 4 VIP potentiates the response of ILC2s and ILC3s to alarmins. **a** After 16 h of fasting, one group of mice remained fasted while another group of mice was refed ad libitum during 3 h before mice were sacrificed and immune cells were isolated. All mice were administered a cocktail of antibiotics prior and during the fasting/refeeding procedure. **b** Production of IL-5 (red) or IL-22 (blue) by intestinal lamina propria cells isolated from fasted and fasted-refed (antibiotic-treated) wild-type mice, after 6 h of culture in control media (unstimulated = UN) or in presence of IL-33 or IL-23. Data are from $n = 3-6$ mice and 2 independent experiments. **c** Production of IL-22 by intestinal lamina propria cells isolated from fed wild-type or ILC3 $^{\Delta VIPR2}$ mice after 6 h of culture in control media (unstimulated = UN) or in presence of IL-23. Data are from $n = 7-9$ mice and 3 independent experiments. **d** Sorted ILCs unstimulated or cultured in presence of alarmin (IL-33 or IL-23) alone, VIP alone, VIP and alarmin, VIP and alarmin preceded by “Antag” treatment, VIP followed by “Antag” treatment and subsequently with alarmin. “Antag” treatment refers to an incubation of ILCs with VIPR2 antagonist PG-99-465 for 10 min. **e** Production of IL-5 (red) or IL-22 (blue) by FACS-sorted intestinal ILC2s or ILC3s in the different culture conditions detailed in **d**. Data are from $n = 3$ independent experiments where cells from 5–7 mice were pooled for each point. Statistical analysis: Student’s *t*-test. ns, not significant; * $P < 0.05$; ** $P < 0.01$; mean \pm s.e.m.

potentiates ILC activity, but poorly induces ILC activity directly. It is the concomitant or subsequent exposure to type 2 or type 3 inducer cytokines that determines activation of ILC2s or ILC3s, revealing a synergy between cytokines and VIP. Thus, VIP unspecifically primes and alerts the immune system of the presence of food, and thus of the potential presence of pathogens, while specific inducer cytokines are produced by the immune system in response to the presence of such pathogens (or pathobionts).

We show that VIP genuinely potentiates, rather than activates, ILCs. Both in vivo and in vitro, exposure of ILCs to VIP can precede exposure to inducer cytokines to retain synergy between VIP and the cytokines. This potentiation effect of VIP may be particularly relevant in the intestine, as food intake will precede, by minutes or hours, the effect of foodborne pathogens. Indeed, we show that CCK (Fig. 3e), produced by enteroendocrine cells sensing the presence of food, induces the release of VIP by the ENS within minutes. Engagement of VIPR2 by VIP leads to increased intracellular levels of cAMP and Ca^{2+} , which in turn is required for the potentiation effect. Furthermore, we find that VIP

potentiates ILCs *via* induction of the glycolysis pathway. This observation supports previous work showing that ILC2s require glucose to engage effector functions^{21,22}. Together with cytokines, VIP also mobilizes mTOR²⁸, a central hub in cellular energy metabolism, which plays a key role in ILC function^{21,23–26}. We therefore propose that VIP potentiates ILCs through multiple, potentially converging routes, involving cAMP and glycolysis. We also show that VIP induces a potentiation that persists in its absence for at least 3 hours, but the exact duration and specificity of this potentiation in ILCs remains to be determined.

From pioneering studies in neuroscience, potentiation is a conceptual framework central to the study of learning mechanisms in both invertebrate and vertebrate nervous systems³⁷. For instance, mounting evidence has implicated the role of the concentration of free cytosolic Ca^{2+} together with the cAMP signaling pathway in several forms of neuroplasticity, including both short- and long-term potentiation³⁸. The late phase of LTP (lasting more than 3 h), which requires protein synthesis, is dependent on mTOR signaling³⁹ and AMPK⁴⁰. Moreover, long-

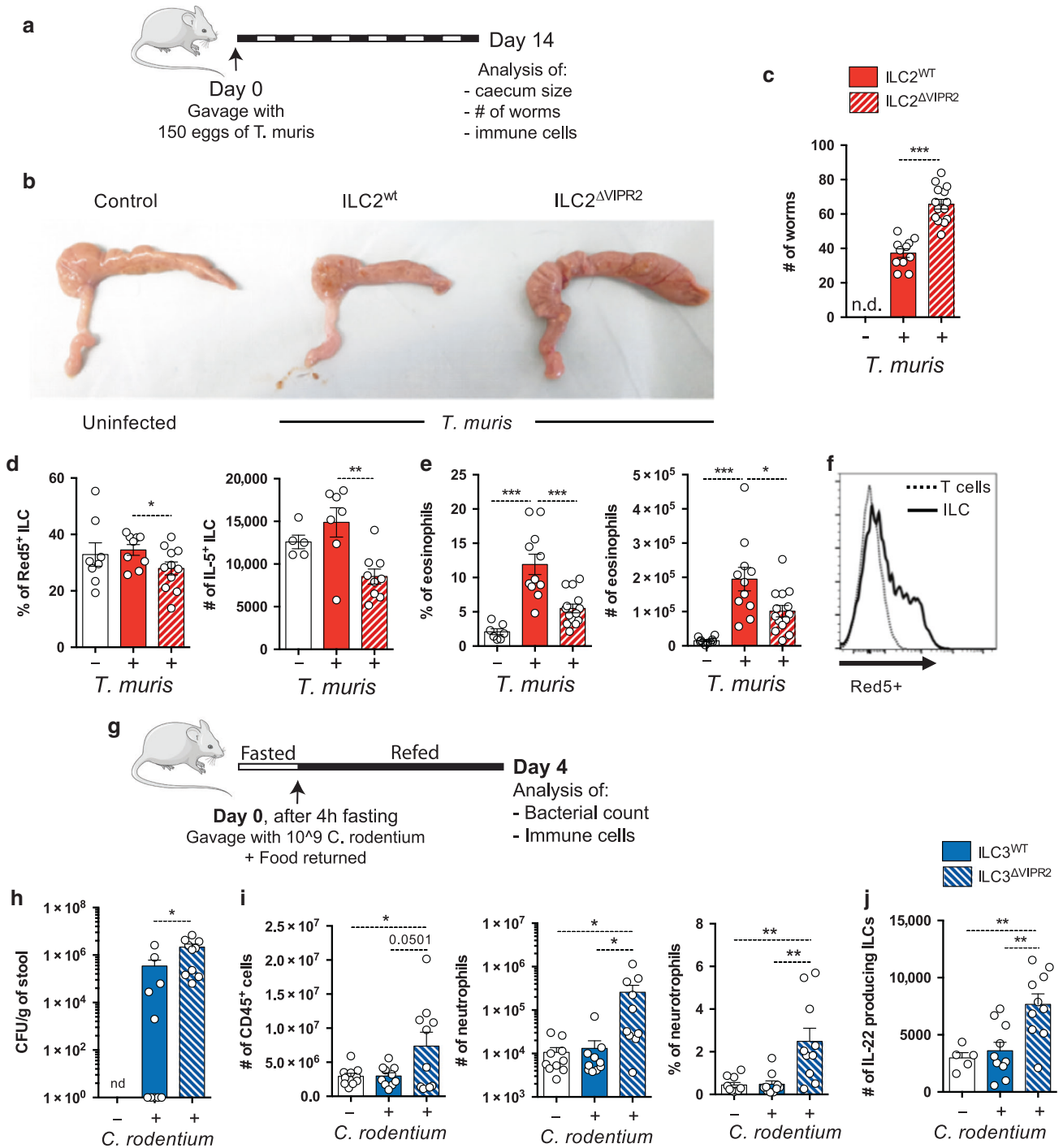


Fig. 5 VIP reinforces type 2 and type 3 ILC-mediated immunity against infection. **a** ILC2^{WT} and ILC2^{ΔVIPR2} mice were infected with 150 eggs of *Trichuris muris*. **b** Representative pictures of cecum harvested at day 14 post infection from control and infected wild-type and ILC2^{ΔVIPR2} mice. **c** Worm burden in the cecum and proximal colon of *T. muris* infected mice. **d** Frequency of Red5⁺ (reporting IL-5 expression) ILCs and number of IL-5 expressing ILCs in the cecum and proximal colon of control and infected ILC2^{WT} and ILC2^{ΔVIPR2} mice. **e** Frequency and number of eosinophils among CD45⁺ cells. **f** Red5⁺ expression in ILCs vs T cells. **g** ILC3^{WT} and ILC3^{ΔVIPR2} mice were infected with *Citrobacter rodentium*. **h** *C. rodentium* burden in stools isolated from the colon of control uninfected and *C. rodentium* infected ILC3^{WT} and ILC3^{ΔVIPR2} mice on day 4 p.i. **i** Numbers of CD45⁺ cells and neutrophils, and frequencies of neutrophils among total CD45⁺ cells, isolated from the cecum and colon of control uninfected and *C. rodentium* infected ILC3^{WT} and ILC3^{ΔVIPR2} mice on day 4 p.i. **j** Number of IL-22 producing ILCs. Data are from at least $n = 3-5$ mice and three independent experiments. Statistical analysis: Student's *t*-test. ns, not significant; * $P < 0.05$; ** $P < 0.01$; mean \pm s.e.m.

term memory formation increases energy consumption⁴¹ and is associated with an elevation in glycolytic activity⁴². In contrast, potentiation of the immune system, and the signaling pathways involved in this process, yet remain to be characterized. Co-

stimulation of lymphocytes, mediated by co-receptors and cytokines, is a key determinant of B and T cell activation⁴³, but time-delayed potentiation is, to the best of our knowledge, poorly described in the immune system. Nevertheless, potentiation of the

immune system by the nervous system appears to be a reasonable mode of crosstalk between the two systems. Indeed, neurons can transfer information in a matter of milliseconds, whereas immune cells require cell-to-cell contacts and the production of cytokines, and thus minutes or more, to exchange information. Therefore, we propose that biochemical storage of short-term memory may operate in immune cells, as it operates in neurons in the form of transitory activation of intracellular signaling and of protein synthesis, which both rely on increased metabolic activity.

ILCs express high levels of VIPR2 that allow them to respond to VIP. A longstanding debate is whether the functions of ILCs are redundant with the functions of T cells. A prominent study in human suggests that immunity is not affected by the absence of ILCs⁴⁴. However, we argue that timing is key in ILC function as compared to T cell function: most significant functions of ILCs have been observed in acute settings (defense against pathogens, acute injury or physiological challenge)^{1,2,45}. Therefore, ILCs are best positioned to respond to prompt signals emanating from the nervous system in the form of neuropeptides. However, it remains to be explored whether resident memory T cells and “innate” T cells can promptly react to inducer cytokines as ILCs do, also react to neuropeptides.

In conclusion, we propose that the nervous system prepares the immune system to potential threats associated with specific environmental cues. In the context of feeding, the ENS promptly releases VIP to enhance digestion, and also to potentiate ILCs, as food may come with threats, such as pathogens or toxins. It is tempting to speculate that other sensory inputs, such as vision and smell, associated with noxious food through an innate or a learned process, may induce enteric production of VIP and potentiation of ILCs, as an anticipatory measure to face such threats. Potentiation of innate immunity by the nervous system may thus have important implications in immunotherapy, as such neuro-immune crosstalk could be targeted to regulate or enhance immunity *via* the manipulation of diverse perceptive modes and cognitive states.

METHODS

Mice

Eight weeks C57BL/6 male and female mice were purchased from Janvier Labs. VIP^{Cre} mice were generously provided by U. Maskos (Institut Pasteur) and bred with Rosa26R^{Yfp/Yfp} mice in order to obtain VIP^{YFP} mice. IL-5^{Cre} × VIPR2^{loxP} (ILC2^{ΔVIPR2}) and RORγt^{Cre} × VIPR2^{loxP} (ILC3^{ΔVIPR2}) mice were generated and maintained in Bonn. Rorc(γt)^{Gfp/+}⁴⁶ and Gata3^{Gfp/+} mice were maintained in our mice facilities. Mice were maintained in the Institut Pasteur or University Hospital Bonn animal facilities under specific pathogen-free conditions and used at 6–12 weeks of age for most experiments. Animal care and experiments were performed according to the committee on animal experimentation of the Institut Pasteur and authorized by the French Ministry of Research or the local and regional ethical committees of the state of North-Rhine-Westfalia.

Fasted/refed procedures and antibiotics treatment

Mice were fasted overnight and remained fasted or were fed ad libitum during 1–3 h the next morning, before deep anesthesia or euthanasia. In some cases, a cocktail of antibiotics listed below (Table 1) was administered in the drinking water starting 24 h before fasting until analysis (See Fig. 3a).

Fasted/continuous feeding procedure

In order to compare our results to ref.¹⁴, a group of mice was fasted overnight (for 16 h before immune cells isolation) and compared to another group of mice which remained fed ad libitum during the whole procedure.

Circadian rhythm experiments

In order to evaluate the impact of circadian rhythms on VIP-induced ILC priming, mice were fasted overnight and remained fasted or were fed ad libitum during 3 h at 4 h of “day time”.

Table 1. List and concentrations of antibiotics.

Antibiotics	Concentrations (g L ⁻¹)	References	Manufacturer
Streptomycin	5	S6601-100G	Sigma-Aldrich
Metronidazole	0.5	M3761-25G	Sigma-Aldrich
Ampicillin	1	A9518-25G	Sigma-Aldrich
Colistin	1	27665-5G	Sigma-Aldrich
Vancomycin	0.5	V1130-5G	Sigma-Aldrich

DREADD-induced VIP release procedure

To transduce peripheral VIP-expressing neurons, we leveraged the capacity of AAV9 viral vectors to transduce peripheral enteric neurons following i.v. injection while sparing brain neurons⁴⁷. Six-week-old VIP-cre mice were injected i.v. in the retro-orbital sinus with AAV9-hSyn-DIO-mCherry (control virus, Addgene #50459; ~5 × 10¹² viral genomes per mouse) or AAV9-hSyn-DIO-hM3D-mCherry (DREADD-Gq virus, Addgene# 44361; ~5 × 10¹² viral genomes per mouse). Three weeks later, mice were fasted overnight. On the next morning, 1 mg/kg of Clozapine-N-Oxide (CNO; Sigma) per mouse was administered i.p. For VIP dosage in the portal vein blood, mice were anesthetized and blood was sample 30 min after CNO injection. For immune cells analysis, mice were sacrificed 3 h after CNO injection.

In vivo treatment with IL-23 and IL-33

ILC2^{WT} and ILC2^{ΔVIPR2} mice were administered 200 ng recombinant IL-33 in PBS or PBS alone *i.p.* at day 0 and day 3. Mice were sacrificed on day 4 post injection. ILC3^{WT} and ILC3^{ΔVIPR2} mice were administered on 3 consecutive days with 200 ng recombinant IL-23 in PBS or PBS alone *i.p.* starting day 0 and sacrificed on day 3. The cecum and proximal colon (IL-33 injected animals) or small intestine (IL-23 injected animals) of injected animals was removed and lymphocytes isolated. Single-cell suspensions were stained and analyzed by flow cytometry.

CCK injection and portal vein blood sampling

Mice were fasted overnight. Cholecystokinin (CCK) (40 μg/kg of mice, Tocris 1166) or PBS was injected *i.p.* Mice were anesthetized using Ketamine/Xylazine (100 mg/kg and 10 mg/kg, *i.p.*) a few minutes before blood collection. Abdominal fur was removed, a midline laparotomy was performed and the gut was moved in order to get access to the portal vein. Samples were collected using an insulin syringe into eppendorf tubes containing EDTA or heparin and aprotinin. Samples were kept on ice until centrifugation and plasma collection.

VIP quantification

Samples analysis was performed by ¹²⁵I radioimmunoassay targeted against C-terminal end of the VIP using the DAsource-VIP-RB311 Kit and a WIZARD Gamma Counters-Perkins Elmer (performed by RIA and Clinical Trials Business Units of Laboratoire de Biologie Spécialisée Eurofins Biomnis 78, avenue de Verdun 94200 Ivry-sur-Seine).

Infection models

Type 2 infectious model. On day 0 ILC2^{WT} and ILC2^{ΔVIPR2} mice were administered 150 eggs of *T. muris* via oral gavage in 200 μl H₂O. Mice were sacrificed on day 14 post infection. The cecum and proximal colon of infected animals was removed and lymphocytes isolated. Single-cell suspensions were stained and analyzed by flow cytometry.

Type 3 infectious model. *C. rodentium* was grown for 3–4 h in 5 ml LB medium until an OD of 0.6, washed and resuspended in PBS prior to infection. On day 0, ILC3^{WT} and ILC3^{ΔVIPR2} mice were fasted for 4 h. After fasting mice were administered 1 × 10⁹ *C. rodentium* via oral gavage in 200 μl PBS at the same time food was returned to the cages. On day 4 post infection mice were sacrificed, followed by lymphocyte isolation from the cecum and proximal colon. Single-cell suspensions were stained and analyzed by flow cytometry.

Isolation of lymphoid cells from small intestine and colon lamina propria

Lamina propria cells were isolated as described previously⁴⁸. Briefly, Peyer's patches were removed, and whole intestine was opened longitudinally, cut

Table 2. Primary and secondary antibodies used for microscopy.

Target	Origin	Reference		Concentration
CD3	Hamster	BD Biosciences	562286	1:500
CGRP	Rabbit	Sigma	C8198	1:1000
GFP	Chicken	Abcam	ab13970	1:500
HuC/D	Mouse	Fischer	A21271	1:80
TUJ1	Mouse	Ozyme	BLE801201	1:500
TUJ1	Rabbit	Cell signaling	D71G9	1:500
VIP	Rabbit	Immunostar	20077	1:500
Secondary antibody		Reference		Concentration
Donkey anti-rabbit 488		Jackson	711-546-152	1:500
Donkey anti-rabbit biotin		Jackson	711-065-152	1:500
Donkey anti-mouse 647		Jackson	715-606-151	1:500
Donkey anti-goat 488		Jackson	705-546-147	1:500
Goat anti-rabbit 568		Millipore	11036	1:500
Goat anti-rabbit 647		Millipore	A21244	1:500
Goat anti-mouse 647		Millipore	21235	1:500
Goat anti-mouse 405		Millipore	A31553	1:500
Goat anti-chicken 488		Life technologies	A11039	1:500

into pieces, incubated for 30 min in 30 mM EDTA, washed extensively, and incubated for several rounds in Liberase TL and DNase. These preparations were then grinded through a 100 µm filter to generate single-cell suspensions, separated by a 40/80% (w/v) Percoll density gradient and washed prior to further manipulation.

Quantitative RT-PCR

Frozen tissue samples (duodenum, ileum) were dissociated, and RNA isolation, cDNA synthesis and purification were performed using the Thermo Pure Link RNA Mini Kit, following the manufacturer's instructions. Real-time quantitative PCR cDNA was performed using SybrGreen (BioRad) and Qiagen primers. Ct values were normalized to the Ct obtained for the pan-neuronal marker Tuj1. Cells were lysed in RLT lysis buffer with 1% 2-mercaptoethanol. RNA isolation was performed using the Microkit Qiagen with DNA carrier, following the manufacturer instructions. cDNA and real-time quantitative PCR were performed using the superscript IV, SybrGreen (BioRad) and Qiagen primers. Ct values obtained for genes of interest in each ILC subtypes were normalized to the Ct obtained for CD4⁺ T cells or the corresponding T cell subset. For analysis of metabolic genes induced by combinations of VIP and IL-23 or IL-33 in ILC2s and ILC3s, TaqMan probes for *hprt1*, *hif1a*, *eno1*, *ldha*, *pkm*, (IDT) were used and target-gene expression was calculated using the comparative method for relative quantification upon normalization to *Hprt1* gene expression.

Immunofluorescence and whole mount histology

Mice were either sacrificed by cervical dislocation or anesthetized using Ketamine/Xylazine (200 mg/kg and 20 mg/kg, i.p.), and transcardially perfused with cold PBS followed by 4% PFA (buffered in PB 0.1 M, pH = 7.4). The small intestine was then harvested and cut open longitudinally and the luminal contents washed away in PBS. The tissue was pinned down into a polystyrene plate and postfixed in 4% PFA for 24 h. After several washes in PBS, samples were transferred in PBS containing 25% sucrose for cryoprotection. For immunostaining of lymphoid cells, 1 cm pieces of duodenum were rolled and frozen prior to the cutting of 100 µm transversal slices using a freezing microtome. For whole mount studies of the myenteric and the submucosal plexuses, the *muscularis externa* was carefully separated from the underlying mucosa and the villi were removed. Samples were permeabilized in 0.25% or 0.5% Triton X-100 for 1–2 h and then blocked for 2 h in 10% BSA/10% Normal Goat Serum or 10% BSA/10% Normal Donkey Serum /0.25% or 0.5% Triton X-100. Antibodies (listed in Table 2) were added to blocking buffer (5% BSA/5% Normal Goat Serum or 5% BSA/5% Normal Donkey Serum/0.25% or 0.5% Triton X-100) at appropriate concentrations and incubated at least overnight at 4 °C. The following day, the tissue was washed 3 times in 1× DPBS and then incubated in blocking buffer with secondary antibodies at appropriate concentrations for 2 h at room temperature. Samples were

again washed 3 times in 1× DPBS and mounted on slides with Fluoromount-G with or without DAPI, cover-slipped, and sealed.

Imaging

Imaging was performed using a confocal laser-scanning microscope (LSM 700, 10× or 40× objective; Zeiss) or a microscope (10× objective) equipped with the Apotome system (Zeiss) and Axiovision 4.8 software (Zeiss).

Image analysis

2D analysis of ILC2/3 and VIP fibers colocalization was performed as follows: (1) Sample analysis was done on individual confocal planes for both GFP and CD3 staining. (2) In order to account for variability of colocalized pixels, we resorted to an oversampling approach in order to average out variabilities. (3) Fluorescence Intensity and cell count approaches were not used. However, selection of thresholded pixels was performed to normalize fluorescence intensity across different markers and samples. (4) A common pixel approach was used: data was selected based on connected pixels with the MATLAB function *bwareopen* with thresholding described above. (5) Contours were defined by MATLAB function *bwboundaries*, and converted to binary signal. (6) Percentage common pixels on both channels were then calculated from the binary sums in each channel. *Eg.* $(\text{Sum}(\text{binary image_marker 1} + 2))/(\text{Sum}(\text{binary image_marker 2}))$. (7) The percentage colocalization was normalized by the sum of the pixel intensities in the boundary defined in step 5.

3D analysis of ILC2/3 and VIP fibers juxtaposition in villi was performed using the Imaris software on images acquired by confocal microscopy (stacks of optical slices (1 µm thick) along the z axis of tissue sections). After creating a surface corresponding to the portion of villi analyzed, a semi-automated tracing of VIP⁺ nerve fibers was performed using the filament tool. GFP⁺ and CD3⁺ cells and were represented as spheres after automated spot detection. The distance from each cell center to the closest fiber edge was then computed. Data are presented as (1) the average distance measured between each type of cells and VIP⁺ fibers edge or (2) as the number of cells for each cell types spotted from 1 to 15 µm from a fiber edge, normalized by the corresponding cell density in each villi analyzed.

Quantitative analysis of VIP expression: (1) Sample analysis was performed on individual confocal planes for both VIP and TUJ1 staining. (2) In order to account for variability of colocalized pixels, we applied an oversampling approach in order to average out variabilities. (3) Selection of thresholded pixels was performed to normalize fluorescence intensity across different markers and samples. (4) A common pixel approach was used: data was selected based on connected pixels using the MATLAB function *bwareopen* with thresholding described above. (5) Contours were defined by MATLAB function *bwboundaries*, and the pixels below the threshold were converted to NaN values. (6) For the pixels above the threshold,

Table 3. List of ELISA kits.

Cytokine	Name of the kit	Reference	Manufacturer
IL-5	Mouse IL-5 Quantikine ELISA Kit	M5000	R&D
IL-13	Mouse IL-13 Culture Media Quantikine ELISA	M1300CB	R&D
IL-17	Mouse IL-17 Quantikine ELISA Kit	M1700	R&D
IL-22	Mouse/Rat IL-22 Quantikine ELISA Kit	M2200	R&D
IL-23	Mouse IL-23 Quantikine ELISA Kit	M2300	R&D
IL-33	Mouse/Rat IL-33 Quantikine ELISA Kit	M3300	R&D

Table 4. List of LEGENDplex.

Cytokine	Name of the kit	Reference	Manufacturer
IL-5	LEGENDplex™ Mouse IL-5 Capture Bead A5, 13X	740056	BioLegend
IL-22	LEGENDplex™ Mouse IL-22 Capture Bead B7, 13X V02	740738	BioLegend
Detection antibodies	LEGENDplex™ Mouse Th Cytokine Detection Antibodies V02	740742	BioLegend

which represented the complete fibers in the image, the mean of their fluorescent intensity was calculated. The same procedure was applied to both VIP and TUJ1, and the ratio of their thresholded mean values was calculated for each image (VIP/TUJ1). A mean intensity for the thresholded VIP signal and the thresholded TUJ1 signal was calculated for the ratio. Each value represents one villus measurement for all the fibers contained in the imaging plane.

Cell culture of lymphoid cells

For cell culture of total lymphoid cells, 0.5×10^6 cells were cultured in 250 μ l RPMI 1640 (Invitrogen) containing 10% FBS, 0.05 mM 2-mercaptoethanol, and 100 U/ml of penicillin and streptomycin at 37 °C with 5% CO₂. Cells were stimulated with IL-23 (10 ng/ml) or IL-33 (10 ng/ml). For cultures of FACS-sorted cells, Rorc(yt)^{Gfp/+} and Gata3^{Gfp/+} mice were used as a source of ILC3s and ILC2s, respectively. Five thousand cells were cultured in 150 μ l RPMI 1640 (Invitrogen), or 10,000 cells in 50 μ l RPMI for experiments performed with VIPR2^{loxP} mice, containing and 10% FBS, 0.05 mM 2-mercaptoethanol, and 100 U/ml of penicillin and streptomycin with IL-7 (10 ng ml⁻¹) and SCF (20 ng ml⁻¹). We tested the effect of different combination of alarmins IL-23 (10 ng/ml) or IL-33 (10 ng/ml), VIP (1 μ M), db-cAMP (1 μ M). BAPTA-AM (10 μ M) + EDTA (1 mM) was used to deplete extracellular and intracellular calcium during a 30 min pre-incubation and washed before further cell stimulation in presence of EDTA (1 mM). For in vitro priming experiments, cells were cultured under conditions presented in Fig. 4d. "Antag" is incubation of ILCs with VIPR2 antagonist PG-99-465 (10 μ M, Tocris) for 10 min (black rectangles).

In vitro deletion of VIPR2 in ILC2

For the generation of ILC2 lacking VIPR2, wild-type or VIPR2^{loxP} ILC2 were cultured in 50 μ l RPMI 1640 (Invitrogen) without FBS, 0.05 mM 2-mercaptoethanol, 25 mM HEPES, sodium pyruvate, minimal essential aminoacids (MEM) and 100 U/ml of penicillin and streptomycin at 37 °C with 5% CO₂ for 2 h, in the presence of 2.5 μ M TAT-Cre (Millipore) and with IL-7 (20 ng ml⁻¹) and SCF (20 ng ml⁻¹). After 2 subsequent washes with PBS, cells were rested in RPMI + 10% FBS in the presence of IL-7 (20 ng ml⁻¹) and SCF (20 ng ml⁻¹), followed by activation with IL-33 (10 ng/ml) with or without VIP (1 μ M).

Restimulation of cells for intracellular cytokine staining

Cells isolated from the lamina propria were stimulated for 3 h with cell stimulation cocktail (1:500, eBioscience) in the presence of brefeldin A (1 mg/ml) (GolgiPlug, BD Biosciences) in IMDM supplemented with 10% FCS. Stimulated cells were stained for surface markers, fixed with 3.75% formaldehyde, permeabilized with 0.1% NP-40 and stained with antibodies for IL-5 and IL-22.

Phospho flow

To stain for phospho-Akt, phospho-mTOR and phospho-S6, isolated intestinal lymphocytes of IL-33 or IL-23 treated mice were seeded in a 96-well U-bottom plate and re-stimulated with both IL-33 (10 ng/ml) and VIP (1 μ M) for ILC2 or IL-23 (10 ng/ml) and VIP (1 μ M) for ILC3 in RPMI

supplemented with 10% FCS for 25 min at 37 °C. Immediately after restimulation, cells were fixed with FOXP3 fixation and permeabilization buffer (ThermoFisher eBioscience) for 20 min, washed and treated with 90% ice-cold methanol for 30 min at 4 °C. Fixed cells were washed and stained for Thy1.2, CD45, CD4, TCRb, GATA3, RORyt, pAkt, pmTOR and pS6 in permeabilization buffer for 60 min at 4 °C.

SCENITH

SILPL were incubated for 30 min at 37 °C, 5% CO₂ followed by treatment for 30 min at 37 °C, 5% CO₂ with control, 2-DG (100 mM (ILC2)), 50 mM (ILC3); Sigma-Aldrich), oligomycin (1 μ M (ILC2)), 0.5 μ M (ILC3); Sigma-Aldrich) or a combination of both drugs. Puromycin (10 μ g ml⁻¹; Abcam) was added for 30 min at 37 °C. After staining with primary antibodies as described above, cells were fixed and permeabilized using the Foxp3 fixation/permeabilization kit (eBioscience) following the manufacturer's instructions. Intracellular staining of puromycin was performed by incubation with the anti-puro monoclonal antibody (1:1000, Clone MABE343, Merck) for 30 min at 4 °C. This protocol was adapted from the original SCENITH kit (<http://www.scenith.com>) and protocols developed by R. Argüello²⁹.

ELISA

IL-5, IL-13, IL-17, IL-22, IL-23, IL-33 quantifications were performed using R&D Mouse Quantikine ELISA kits, on culture supernatant or plasma samples, following to the manufacturer instructions (Table 3).

Bead-based multiplex assay (LEGENDplex)

For the conditional VIPR2 knock-out experiments with VIPR2^{loxP} mice, a bead-based cytokine quantification assay was used according to the manufacturers' protocol (Table 4).

Fluorescence activated cell sorting of lymphoid cells

Lamina propria lymphoid cells isolated from GATA3^{GFP} or RORyt^{GFP} mice were pre-incubated with Fc-Block for 10 min and stained for 20 min with antibodies to surface markers. DAPI was added before sorting in order to differentiate and exclude dead cells. Cells were sorted in OptiMEM as DAPI⁻CD45⁺CD3⁻CD19⁻CD127⁺GFP⁺ (Supplementary Fig. 10). After sorting, cells were transferred into RPMI 1640 (Invitrogen) containing and 10% FBS, 0.05 mM 2-mercaptoethanol, and 100 U/ml of penicillin and streptomycin prior to stimulation. For experiments performed with VIPR2^{loxP} mice, cells were sorted in RPMI + 10% FCS as DAPI⁻CD45⁺, Lin⁻ (CD3⁻CD19⁻CD11b⁻CD11c⁻TER119⁻DX5⁻NK1.1⁻Gr-1⁻), Thy1.2⁺KLRG-1⁺ for ILC2s or KLRG-1⁻CD127⁺ for ILC3s. After sorting, cells were cultured in RPMI 1640 (Invitrogen) containing and 10% FBS, 0.05 mM 2-mercaptoethanol, 25 mM HEPES, sodium pyruvate, minimal essential aminoacids (MEM) and 100 U/ml of penicillin and streptomycin prior to stimulation.

Flow cytometry analysis

Single-cell suspensions were first treated with anti-CD16/32 (eBioscience), and subsequently with fluorochrome-conjugated antibodies against

Table 5. Antibodies used for flow cytometry.

Antibody	Reference	
CD11c-biotin	Biolegend	117304
CD11b-biotin	Biolegend	101204
CD127-PE	Biolegend	135010
CD127-PE-Cy7	Sony	1275070
Gr-1-biotin	Biolegend	108404
CD19-biotin	Biolegend	115504
CD3-biotin	Biolegend	100304
CD3-APC	eBioscience	17-0031-82
CD4-BV605	BD Pharmingen	560077
CD45-APC Fire 750	Biolegend	103154
CD45.2 V500	BD Pharmingen	563151
CD90.2-BV605	Biolegend	140318
CD90.2-PE-Cy7	eBioscience	25-0902-82
DX5-biotin	Biolegend	108904
GATA3-FITC	BD Pharmingen	560077
IL-22-APC	eBioscience	17-7222-82
IL-22-PE	Biolegend	516404
IL-5-PE	Biolegend	504304
IL-5-APC	Biolegend	504305
Ki67-PE-Cy7	eBioscience	25-5698-82
KLRG-1-Biotin	eBioscience	13-5893
KLRG-1-PerCP-eFluor710	eBioscience	
Ly6G-FITC	Biolegend	127606
NK1.1	Biolegend	108704
ROR γ t-PE	eBioscience	12-6981-82
SA-eF450	eBioscience	48-4317-82
SA-BV421	Biolegend	405225
SA-PE-Texas Red	BD Pharmingen	562284
SiglecF-PE	BD Pharmingen	552126
TER119-biotin	Biolegend	116204
Zombie UV Fixable Viability Kit	Biolegend	423108

markers listed in Table 5. Prior to fixation, Zombie UV Fixable Viability Kit (Biolegend) was used to exclude dead cells as well as SA-eF450 to exclude surface biotin⁺ cells. For examination of transcription factors and cellular proliferation, cells were subsequently treated with the Foxp3 fixation/permeabilization kit (eBioscience) in accordance with the manufacturer's instructions and stained for 30 min at 4 °C with fluorochrome-conjugated antibodies against ROR γ t and GATA3, and analyzed by flow cytometry.

Statistics

Results are shown as mean \pm s.e.m. Statistical analysis was performed with GraphPad Prism software (GraphPad Software version 6.01). Student's *t*-test was performed on homoscedastic populations. Unpaired *t*-test was applied on samples with different variances. Results were considered significant at **P* < 0.05, ***P* < 0.01, ****P* < 0.001.

REFERENCES

- Vivier, E. et al. Innate lymphoid cells: 10 years on. *Cell* **174**, 1054–1066 (2018).
- Eberl, G., Colonna, M., Di Santo, J. P. & McKenzie, A. N. Innate lymphoid cells: a new paradigm in immunology. *Science* **348**, aaa6566 (2015).
- Cardoso, V. et al. Neuronal regulation of type 2 innate lymphoid cells via neuromedin U. *Nature* **549**, 277–281 (2017).
- Klose, C. S. N. et al. The neuropeptide neuromedin U stimulates innate lymphoid cells and type 2 inflammation. *Nature* **549**, 282–286 (2017).
- Wallrapp, A. et al. The neuropeptide NMU amplifies ILC2-driven allergic lung inflammation. *Nature* **549**, 351–356 (2017).
- Nussbaum, J. C. et al. Type 2 innate lymphoid cells control eosinophil homeostasis. *Nature* **502**, 245–248 (2013).
- Talbot, S. et al. Silencing nociceptor neurons reduces allergic airway inflammation. *Neuron* **87**, 341–354 (2015).
- Xu, H. et al. Transcriptional atlas of intestinal immune cells reveals that neuropeptide alpha-CGRP modulates group 2 innate lymphoid cell responses. *Immunity* **51**, 696–708 (2019). e699.
- Nagashima, H. et al. Neuropeptide CGRP limits group 2 innate lymphoid cell responses and constrains type 2 inflammation. *Immunity* **51**, 682–695 (2019). e686.
- Wallrapp, A. et al. Calcitonin gene-related peptide negatively regulates alarmin-driven type 2 innate lymphoid cell responses. *Immunity* **51**, 709–723 (2019). e706.
- Ibiza, S. et al. Glial-cell-derived neuroregulators control type 3 innate lymphoid cells and gut defence. *Nature* **535**, 440–443 (2016).
- Godinho-Silva, C. et al. Light-entrained and brain-tuned circadian circuits regulate ILC3s and gut homeostasis. *Nature* **574**, 254–258 (2019).
- Talbot, J. et al. Feeding-dependent VIP neuron-ILC3 circuit regulates the intestinal barrier. *Nature* **579**, 575–580 (2020).
- Seillet, C. et al. The neuropeptide VIP confers anticipatory mucosal immunity by regulating ILC3 activity. *Nat. Immunol.* **21**, 168–177 (2020).
- Reid, A. M., Shulkes, A. & Titchener, D. A. Gastric and intestinal release of vasoactive intestinal polypeptide in the milk-fed lamb. *Regul. Pept.* **12**, 43–50 (1985).
- Uvnas-Moberg, K. Release of gastrointestinal peptides in response to vagal activation induced by electrical stimulation, feeding and suckling. *J. Auton. Nerv. Syst.* **9**, 141–155 (1983).
- Bitar, K. N. & Makhlof, G. M. Relaxation of isolated gastric smooth muscle cells by vasoactive intestinal peptide. *Science* **216**, 531–533 (1982).
- Schwartz, C. J., Kimberg, D. V., Sheerin, H. E., Field, M. & Said, S. I. Vasoactive intestinal peptide stimulation of adenylate cyclase and active electrolyte secretion in intestinal mucosa. *J. Clin. Investig.* **54**, 536–544 (1974).
- Yu, H. B. et al. Vasoactive intestinal peptide promotes host defense against enteric pathogens by modulating the recruitment of group 3 innate lymphoid cells. *Proc. Natl. Acad. Sci. USA* **118**, e2106634118 (2021).
- Xia, M., Sreedharan, S. P. & Goetzl, E. J. Predominant expression of type II vasoactive intestinal peptide receptors by human T lymphoblastoma cells: transduction of both Ca²⁺ and cyclic AMP signals. *J. Clin. Immunol.* **16**, 21–30 (1996).
- Karagiannis, F. et al. Lipid-droplet formation drives pathogenic group 2 innate lymphoid cells in airway inflammation. *Immunity* **52**, 620–634 e626 (2020).
- Wilhelm, C., Kharabi Masouleh, S. & Kazakov, A. Metabolic regulation of innate lymphoid cell-mediated tissue protection-linking the nutritional state to barrier immunity. *Front Immunol.* **8**, 1742 (2017).
- Monticelli, L. A. et al. Arginase 1 is an innate lymphoid-cell-intrinsic metabolic checkpoint controlling type 2 inflammation. *Nat. Immunol.* **17**, 656–665 (2016).
- Di Luccia, B., Gilfillan, S., Cella, M., Colonna, M. & Huang, S. C. ILC3s integrate glycolysis and mitochondrial production of reactive oxygen species to fulfill activation demands. *J. Exp. Med.* **216**, 2231–2241 (2019).
- Salmond, R. J. et al. IL-33 induces innate lymphoid cell-mediated airway inflammation by activating mammalian target of rapamycin. *J. Allergy Clin. Immunol.* **130**, 1159–1166 (2012). e1156.
- Zheng, C., Wu, H., Lu, Z., Bi, J. & Wan, X. IL-33-induced reactive oxygen species are required for optimal metabolic programming in group 2 innate lymphoid cells. *Cell Mol. Immunol.* **17**, 1266–1268 (2020).
- Maxwell, R. J., Prysor-Jones, R. A., Jenkins, J. S. & Griffiths, J. R. Vasoactive intestinal peptide stimulates glycolysis in pituitary tumours; ¹H-NMR detection of lactate in vivo. *Biochim Biophys Acta* **968**, 86–90 (1988).
- Merech, F. et al. Vasoactive Intestinal Peptide induces glucose and neutral amino acid uptake through mTOR signalling in human cytotrophoblast cells. *Sci. Rep.* **9**, 17152 (2019).
- Arguello, R. J. et al. SCENITH: a flow cytometry-based method to functionally profile energy metabolism with single-cell resolution. *Cell Metab.* **32**, 1063–1075 (2020). e1067.
- Owyang, A. M. et al. Interleukin 25 regulates type 2 cytokine-dependent immunity and limits chronic inflammation in the gastrointestinal tract. *J. Exp. Med.* **203**, 843–849 (2006).
- Humphreys, N. E., Xu, D., Hepworth, M. R., Liew, F. Y. & Grecnis, R. K. IL-33, a potent inducer of adaptive immunity to intestinal nematodes. *J. Immunol.* **180**, 2443–2449 (2008).
- Conlin, V. S. et al. Vasoactive intestinal peptide ameliorates intestinal barrier disruption associated with *Citrobacter rodentium*-induced colitis. *Am. J. Physiol. Gastrointest. Liver Physiol.* **297**, G735–G750 (2009).
- Ivanov, I. I. et al. Induction of intestinal Th17 cells by segmented filamentous bacteria. *Cell* **139**, 485–498 (2009).

34. Gaboriau-Routhiau, V. et al. The key role of segmented filamentous bacteria in the coordinated maturation of gut helper T cell responses. *Immunity* **31**, 677–689 (2009).
35. Ohnmacht, C. et al. The microbiota regulates type 2 immunity through RORγt+ T cells. *Science* **349**, 989–993 (2015).
36. Eberl, G. Immunity by equilibrium. *Nat. Rev. Immunol.* **16**, 524–532 (2016).
37. Malenka, R. C. & Bear, M. F. LTP and LTD: an embarrassment of riches. *Neuron* **44**, 5–21 (2004).
38. Sanes, J. R. & Lichtman, J. W. Can molecules explain long-term potentiation? *Nat. Neurosci.* **2**, 597–604 (1999).
39. Gureev, A. P., Popov, V. N. & Starkov, A. A. Crosstalk between the mTOR and Nrf2/ARE signaling pathways as a target in the improvement of long-term potentiation. *Exp. Neurol.* **328**, 113285 (2020).
40. Potter, W. B. et al. Metabolic regulation of neuronal plasticity by the energy sensor AMPK. *PLoS ONE* **5**, e8996 (2010).
41. Placais, P. Y. et al. Upregulated energy metabolism in the Drosophila mushroom body is the trigger for long-term memory. *Nat. Commun.* **8**, 15510 (2017).
42. Magistretti, P. J. & Allaman, I. Lactate in the brain: from metabolic end-product to signalling molecule. *Nat. Rev. Neurosci.* **19**, 235–249 (2018).
43. Schwartz, R. H. Costimulation of T lymphocytes: the role of CD28, CTLA-4, and B7/BB1 in interleukin-2 production and immunotherapy. *Cell* **71**, 1065–1068 (1992).
44. Vely, F. et al. Evidence of innate lymphoid cell redundancy in humans. *Nat. Immunol.* **17**, 1291–1299 (2016).
45. Cording, S., Medvedovic, J., Lecuyer, E., Aychek, T. & Eberl, G. Control of pathogens and microbiota by innate lymphoid cells. *Microbes Infect.* **20**, 317–322 (2018).
46. Lochner, M. et al. In vivo equilibrium of proinflammatory IL-17+ and regulatory IL-10+ Foxp3+ RORγt+ T cells. *J. Exp. Med.* **205**, 1381–1393 (2008).
47. Chan, K. Y. et al. Engineered AAVs for efficient noninvasive gene delivery to the central and peripheral nervous systems. *Nat. Neurosci.* **20**, 1172–1179 (2017).
48. Sawa, S. et al. RORγt+ innate lymphoid cells regulate intestinal homeostasis by integrating negative signals from the symbiotic microbiota. *Nat. Immunol.* **12**, 320–326 (2011).

ACKNOWLEDGEMENTS

We thank all members of the Microenvironment and Immunity unit, the Perception and Memory unit, and the Stroma, Inflammation and Tissue Repair unit, in particular Bernadette Polomack for mouse genotyping. We also thank Uwe Maskos, Fani Koukoulis and David Digregorio for providing us VIP^{Cre} Mice, and Meinrad Busslinger for the Gata3^{GFP} mice. We thank Pierre Bost for sharing its expertise on image analysis, Jacques Serizay for providing guidance in data visualization for Fig. 1,

Christelle Ganneau and Sylvie Bay for sharing their expertise on peptides biochemistry as well as Martine Jacob and Catherine Fayolle for their precious technical support with mice. M.P. is a recipient of a fellowship from the French Ministère de l'Éducation Nationale et de la Recherche. This work was supported by Institut Pasteur, a seed grant from the Institut Pasteur Strategic Research Axis 3, INSERM, CNRS, the life insurance company "AG2R-La-Mondiale" and grant ANR-16-CE15-0021-01 from the Agence Nationale de la Recherche Scientifique. C.W. and A.K. were funded by the Deutsche Forschungsgemeinschaft (DFG, German Research Foundation) under Germany's Excellence Strategy – EXC2151 – 390873048 and program grants from the DFG (SPP1937, WI 4554/1-1 and WI 4554/1-2).

AUTHOR CONTRIBUTIONS

M.P., conceptualization, methodology, validation, formal analysis, investigation, writing—original draft, writing - review & editing, visualization, supervision; A.K., methodology, validation, formal analysis, investigation, review & editing, visualization; G.C., conceptualization, methodology, investigation; L.D., J.D., A.D., F.J., S.D., C.M., investigation; S.S., K.S., formal analysis; Y.B., resources; G.L., conceptualization, methodology, investigation, writing - original draft, writing—review & editing, supervision, funding acquisition; P.-M.L., C.W., conceptualization, methodology, writing—original draft, writing—review & editing, supervision, funding acquisition; G.E., conceptualization, methodology, writing—original draft, writing—review & editing, project administration, funding acquisition.

COMPETING INTERESTS

G.E. is a deputy editor at *Mucosal Immunology*.

ADDITIONAL INFORMATION

Supplementary information The online version contains supplementary material available at <https://doi.org/10.1038/s41385-022-00516-9>.

Correspondence and requests for materials should be addressed to Maud Pascal, Pierre-Marie Lledo or Gérard Eberl.

Reprints and permission information is available at <http://www.nature.com/reprints>

Publisher's note Springer Nature remains neutral with regard to jurisdictional claims in published maps and institutional affiliations.